

# Active optics and modified-Rumsey wide-field telescopes: MINITRUST demonstrators with vase- and tulip-form mirrors

G rard R. Lema tre, Pierre Montiel, Patrice Jouli , Kjetil Dohlen, and Patrick Lanzoni

Wide-field astronomy requires the development of larger aperture telescopes. The optical properties of a three-mirror modified-Rumsey design provide significant advantages when compared to other telescope designs: (i) at any wavelength, the design has a flat field and is anastigmatic; (ii) the system is extremely compact, i.e., it is almost four times shorter than a Schmidt. Compared to the equally compact flat-field Ritchey-Chr tien with a doublet-lens corrector, as developed for the Sloan digital sky survey—and which requires the polishing of six optical surfaces—the proposed modified-Rumsey design requires only a two-surface polishing and provides a better imaging quality. All the mirrors are spheroids of the hyperboloid type. Starting from the classical Rumsey design, it is shown that the use of all eight available free parameters allows the simultaneous aspherization of the primary and tertiary mirrors by active optics methods from a single deformable substrate. The continuity conditions between the primary and the tertiary hyperbolizations are achieved by an intermediate narrow ring of constant thickness that is not optically used. After the polishing of a double vase form in a spherical shape, the primary-tertiary hyperbolizations are achieved by *in situ* stressing. The tulip-form secondary is hyperbolized by stress polishing. Other active optics alternatives are possible for a space telescope. The modified-Rumsey design is of interest for developing large space- and ground-based survey telescopes in UV, visible, or IR ranges, such as currently demonstrated with the construction of identical telescopes MINITRUST-1 and -2,  $f/5 - 2^\circ$  field of view. Double-pass optical tests show diffraction-limited images.   2005 Optical Society of America

OCIS codes: 080.3620, 220.0220, 220.4610, 350.1260.

## 1. Introduction: Active Optics Methods

Active optics methods applied to the design and construction of optical mirrors are particularly interesting because they naturally provide smooth and accurate optical surfaces. Compared with conventional methods of generating aspherics, active optics avoids the zonal defects of slope discontinuities—i.e., high spatial frequency errors—inherent in the use of local polishing tools. Active methods also provide accurate nonaxisymmetrical optics<sup>1,2</sup> from the vase and meniscus forms. Current applications and developments of active optics are in the following fields:

- (i) Large amplitude aspherization of optics by stress polishing and/or by *in situ* stressing<sup>3–10</sup>;
- (ii) *in situ* compensation of large telescope mirrors due to their deflection in field gravity<sup>11–13</sup>;
- (iii) availability of a variable asphericity for telescopes with multiple foci selected by mirror interchanging<sup>4,5</sup>;
- (iv) field compensation and cophasing of optical telescope arrays by variable curvature mirrors<sup>5,7</sup>;
- (v) segments and diffraction gratings aspherized by replication techniques from active submasters<sup>4–6</sup>;
- (vi) mirror concepts using the superposition of optical modes for adaptive optics systems.<sup>1,2</sup>

## 2. Optical Design of the Modified-Rumsey Telescope

The three-mirror telescope discovered by Rumsey<sup>14</sup> in the 1960s led us to the proposal of a small three-reflection ultraviolet survey telescope (MINITRUST). This compact combination (Fig. 1E) provides flat  $2^\circ$ – $2.5^\circ$  fields of view (FOVs). Compared with other wide-field designs, the overall length of the Rumsey is almost four times shorter than a Schmidt (Fig. 1A),

---

The authors are with the Marseille Provence Astronomical Observatory (OAMP), 2 Place Le Verrier, F-13248 Marseille CX4, France. G. R. Lema tre's e-mail address is gerard.lemaitre@oamp.fr.

Received 4 March 2005; revised manuscript received 20 May 2005; accepted 23 May 2005.

0003-6935/05/347322-11\$15.00/0

  2005 Optical Society of America

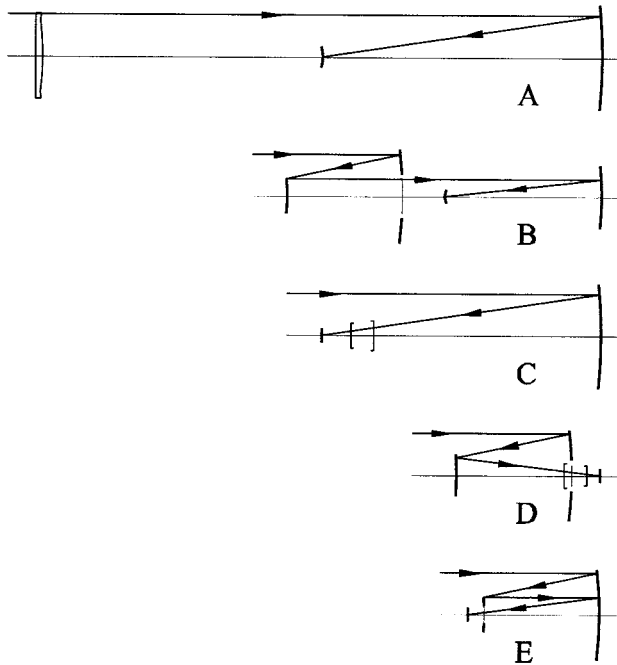


Fig. 1. Comparison of wide-field telescopes having an identical input beam diameter, focal length, and field of view ( $2^\circ$ ): A, Schmidt with refractive corrector—convex FOV, 1 aspheric, length  $\approx 2F$ , 3 polished surfaces; B, Mersenne-Schmidt by Willstrop—concave FOV, 2 aspherics, length  $\approx F$ , 3 polished surfaces; C, paraboloid and triplet-lens corrector—flat FOV, 1 aspheric, length  $= F$ , 7 polished surfaces; D, Ritchey-Chrétien + doublet corrector—flat FOV, 2 aspherics, length  $\approx F/2$ , 6 polished surfaces; E, modified-Rumsey continuous  $M_1$ - $M_3$ —flat FOV, 3 aspherics, length  $\approx F/2$ , 2 polished surfaces.

and two times shorter than the Mersenne-Schmidt proposed by Willstrop<sup>15</sup> (Fig. 1B). The convex field of Schmidts is limited in wavelength range by the chromatic variation of spherical aberration while the Schmidts with a field flattener lens are more limited because of additional lateral chromatism; these systems require the polishing of three or five optical surfaces; one surface is aspheric. With Willstrop systems, the anastigmatism is achieved by an afocal Mersenne pair  $M_1$ - $M_2$ , where  $M_1$  is a paraboloid, and where a Schmidt-type spherical mirror  $M_3$  transfers its spherical aberration onto  $M_2$ , which is at its center of curvature; this system has a small but concave field curvature and requires the polishing of three optical surfaces; two surfaces are aspherics. Designs that use a paraboloid primary with a triplet- or quadruplet-lens corrector (Fig. 1C) are not sufficient for the currently considered  $2^\circ$ - $2.5^\circ$  fields and large spectral ranges down to the atmospheric ultraviolet cutoff; it would require the polishing of seven or nine optical surfaces. A field-extended Ritchey-Chrétien form with a doublet-lens corrector—where the two mirrors are of the same curvature for a flat field (Fig. 1D)—is currently built into a 2.5 m aperture telescope at  $f/2.5/5$  for the Sloan digital sky survey (SDSS) operating at the Apache Point Observatory, New Mexico; the length of this latter form is about

half of the focal length of the primary, which is similar to the present length of the modified-Rumsey design. However, it requires the polishing of six optical surfaces instead of only two surfaces for the present design (see Sections 3 and 4).

In elaborating the complete third-order aberration theory of two-mirror telescopes, Schwartzchild found that the only possible case for a flat-field anastigmat is with a convex primary, and he definitively demonstrated that no such telescope exists with a concave primary. The third-order theory applied to three mirror telescopes was pioneered by Paul,<sup>16</sup> who derived the basic features for anastigmatic systems. Angel *et al.*<sup>17</sup> proposed a Paul system for a survey with charge-coupled devices (CCDs). Small off-axis, three-mirror telescopes have been investigated and built by Dohlen *et al.*<sup>18</sup> for *in situ* comet observations with the Rosetta mission; this centered system at  $f/7$  and  $3^\circ$  flat FOV was developed in a telecentric form.

In presenting his three-mirror design, Rumsey<sup>14</sup> emphasized that the primary and tertiary on a single disk of glass would provide the advantages of a permanently perfect alignment of the tertiary and less diffraction light by avoiding a spider support. Although he stated that the primary and tertiary surfaces together can form a “continuous reflecting surface” without referring to active optics, this may be understood as two mirrors having the sag continuity but separately polished on the same substrate. With both the sag and the slope continuities between the  $M_1$  inner aperture and the  $M_3$  outer aperture, active optics methods would provide many advantages. The best possible active concept allows the simultaneous aspherization of the  $M_1$  and  $M_3$  mirrors. This would use only a full aperture polishing tool (of spherical shape), provided the elasticity conditions with convenient thickness distributions can be satisfied for generating the two mirrors simultaneously.

It has been found that an intermediate narrow ring of convenient constant axial thickness, not used optically, between the  $M_1$  and the  $M_3$  mirrors provides the sag and slope continuity conditions. This defines a modified-Rumsey design having the following features:

- (a)  $M_1$  and  $M_3$  mirrors are generated from a single deformable substrate with four concentric rigidity zones in a double vase form. Two of these rigidities vary slightly from the center to the edge when corresponding to the clear aperture of the mirrors.
- (b) The elastic aspherizations are both obtained by a single constant uniform loading in reaction at the edge of the two-mirror substrate.
- (c) The optical surfacing alternatives for the  $M_1$  and  $M_3$  mirrors are a stress polishing at the laboratory or an *in situ* stressing at the telescope.
- (d) The present process uses the equivalent of polishing only one surface in making two concentric mirrors.

The optics third-order theory with three mirror

Table 1. Modified-Rumsey Design of MINITRUST-f/4.9-2° FOV- $\lambda\lambda$ [380–900 nm]

$i$	Surface	$R_i$	$z_{Si}$	$D_i$	$E_i$	Clear Aperture	$[\kappa_i]^\alpha$
1	Primary	-2208.0	-630.000	$6.3905 \times 10^{-12}$	$3.1327 \times 10^{-19}$	440	[-1.550]
2	Secondary	-1096.0	630.005	$2.7995 \times 10^{-10}$	$-2.4184 \times 10^{-16}$	Stop 200	[-3.948]
3	Tertiary	-2197.2	-763.403	$7.5810 \times 10^{-11}$	$-6.9152 \times 10^{-17}$	180	[-7.433]
4	Fused	$\infty$	-10.000			$59 \times 59$	
5	Silica	$\infty$	-25.000			$58 \times 58$	
6	Focus	$\infty$				$56 \times 56$	

Note: Equation of mirrors:  $z_i = (1/2R_i)r^2 + D_i r^4 + E_i r^6$ . Axial separations:  $z_{Si}$ . Continuity of slopes and sags of  $M_1$  and  $M_3$  realized at  $r = 90$  mm. Dimensions in mm.

<sup>a</sup>Equivalent conic constant in third order:  $\kappa_i = 8R_i^3 D_i - 1$  ( $\kappa = -1$  for a paraboloid).

telescopes allows eight parameters: three curvatures, three conic constants, and two axial separations. A flat-fielded anastigmat requires the aberration correction  $S_{p3} = C_{oma3} = A_{stm3} = 0$  and zeroing Petzval curvature  $Petz3 = 0$ . For a Rumsey, we also require the curvatures  $c_1 \approx c_3$ , axial separations  $z_{S1} \approx -z_{S2}$  (allowing the same substrate for  $M_1$  and  $M_3$ ), and a convenient separation  $z_{S3}$  of the focal plane, that is, seven parameters. In addition, a modified-Rumsey for a simultaneous aspherization of  $M_1$ – $M_3$  mirrors by active optics requires a slope continuity of  $z_1' = z_3'$  at the intermediate optical height, thus using the remaining parameter:

Given a focal scale and  $f$  ratio, there is one and only one modified-Rumsey design that satisfies all the conditions.

With the third-order aberration theory, all mirrors are of the hyperboloid type with conic constants increasing from the primary to the tertiary. The optical design of MINITRUST has been carried out with the eight optics parameters restricted by all previous conditions. A pupil of 200 mm aperture defined the secondary clear aperture and an axial separation of  $z_{S1} = 630$  mm provided a focal length of  $F = 2257$  mm; the system  $f$  ratio is  $f/4.9$  (Table 1, Figs. 2 and 3).

In addition, the aspherization of the convex secondary mirror was carried out by stress polishing (see Section 4). This holed mirror is also a spheroid of the hyperboloid type. We have developed, for the first time to our knowledge, a substrate geometry using a

tulip form with its rear central part cut into a large finite thickness; hence the whole optical aperture of the mirror is built into a thick inner ring. In this elasticity design, the middle surface corresponding to the clear aperture is a quasi-plane; hence accurate deformations were derived from the basic thin plate elasticity theory in operating a spherical surfacing with controlled partial vacuum.

Configuring the three mirrors using the classical controlled-retouch method would have been a difficult task, with no guarantee that it would avoid high spatial frequency errors due to zonal tools. These manufacturing difficulties explain the reasons no such telescope has been built yet despite their compactness. Active optics methods that have been developed at the optical laboratory (LOOM) since the 1970s allow for a drastic change in the situation. For present telescopes, this provides the great advantage of polishing only two surfaces that are spheres.

### 3. Elasticity Design of the $M_1$ – $M_3$ Double Vase Form by *In Situ* Stressing

When considering a vase form, defined as a meniscus strengthened by a perimeter ring, it has been shown that, except for few singular cases, the active aspherization of a spherical surface can generate optical spheroids.<sup>19,20</sup>

Given a material and a uniform load applied under the mirror surface in a perimeter reaction, the problem is to determine, in a cylindrical coordinate frame ( $z, r$ ), the mirror substrate geometry—with its thickness distribution  $t(r)$ —providing the optical surface

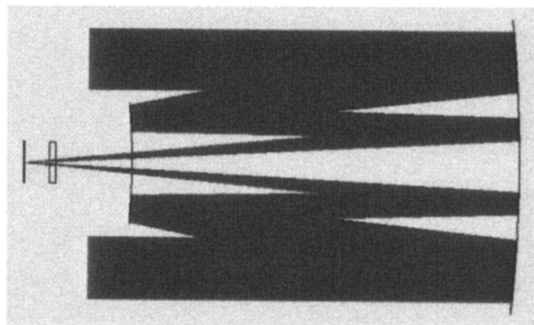


Fig. 2. MINITRUST layout with on-axis beams.

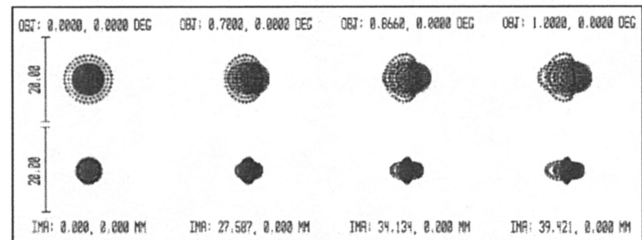


Fig. 3. Residual blur images from Table 1 parameters. 2° FOV,  $\lambda\lambda$  (380–900 nm), and window-filter flat plate. Top, 10 mm thick plate; bottom, 5 mm thick plate. Barr = 20  $\mu$ m. Spherochromatism of plates dominate.

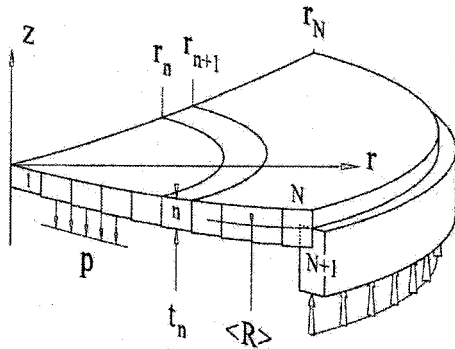


Fig. 4. Geometric parameters of an element ring.

from a coaddition of the flexure to the spherical polished surface. The elasticity analysis is carried out with the theory of shallow shells applied to a vase form. The thickness distribution  $\{t_1, \dots, t_n, \dots, t_N\}$  of  $N$  concentric rings is solved by using the continuity conditions that allow passing from ring  $n$  to the next ring,  $n + 1$  (Fig. 4).

The following notation is used for the shell analysis with a distribution of concentric segments:  $E$  is Young's modulus;  $\nu$  is Poisson's ratio;  $\langle R \rangle$  is the radius of curvature of the middle surface;  $p$  is the intensity of the external uniform load;  $t_n$  is the orthogonal thickness of the element ring;  $D_n$  is the rigidity of the element ring;  $l_n$  is the characteristic length of the element ring.

$$D_n = Et_n^3/[12(1 - \nu^2)], \quad l_n = \sqrt{\langle R \rangle t_n / \sqrt{12(1 - \nu^2)}}. \quad (1)$$

We consider segments continuously distributed along a spherical middle surface before loading with the assumption of shallowness, i.e., where the maximum slope of the middle surface is much lower than unity,

$$\left(\frac{dz}{dr}\right)_{\max} \approx \frac{r_{\max}}{\langle R \rangle} \ll 1. \quad (2)$$

From the Reissner theory of shells,<sup>21,22</sup> the normal and tangential displacements  $w(r)$  and  $u(r)$  of element ring number  $n$ , of constant thickness  $t_n$  extending from current radius  $r_n$  to radius  $r_{n+1}$ , is obtained by the coaddition of two functions that are respective solutions of two differential equations. In the present case, where a continuous uniform load applied to each ring element is considered, one of the six integration coefficients  $C_{i,n}$  in the general expression of  $w$  vanishes; thus the deformation can be represented by

$$w(r) = l_n[C_{1,n}\psi_1(x) + C_{2,n}\psi_2(x) + C_{3,n}\psi_3(x) + C_{4,n}\psi_4(x) + C_{5,n}], \quad (3a)$$

$$u(r) = rF(\psi_i', \psi_i'', p) + rw/\langle R \rangle, \quad (3b)$$

where

$$x = r/l_n, \quad (3c)$$

and where  $F$  is a function of the four  $\psi_i$  first and second derivatives, and the load  $p$ . Denoting  $\nabla^2 \cdot = d^2 \cdot / dr^2 + (1/r)d \cdot / dr$  the Laplacian with respect to current radius, and considering the real and imaginary components of the zero-order Bessel functions (Refs. 23 and 24)  $I_0(\sqrt{i}r/l_n)$  and  $K_0(\sqrt{i}r/l_n)$ , we obtain the following zero-order Kelvin functions:

$$\begin{aligned} \psi_1 &= \text{ber}(r/l_n), & \psi_2 &= \text{bei}(r/l_n), \\ \psi_3 &= \text{ker}(r/l_n), & \psi_4 &= \text{kei}(r/l_n), \end{aligned} \quad (4)$$

which are independent solutions of one of the two equations of shells, namely,

$$\nabla^2 \nabla^2 \psi_i + \frac{1}{l_n^4} \psi_i = 0. \quad (5)$$

The Kelvin functions  $\psi_i(x) \equiv \psi_i(r/l_n)$  are represented by the series<sup>22,23</sup>

$$\text{ber } x = 1 - \frac{(x^2/4)^2}{(2!)^2} + \frac{(x^2/4)^2}{(4!)^2} - \dots, \quad (6a)$$

$$\text{bei } x = \frac{x^2/4}{(1!)^2} - \frac{(x^2/4)^3}{(3!)^2} + \frac{(x^2/4)^5}{(5!)^2} - \dots, \quad (6b)$$

$$\begin{aligned} \text{ker } x &= -\left[\ln\left(\frac{x}{2}\right) + \gamma\right] \text{ber } x + \frac{\pi}{4} \text{bei } x \\ &\quad - \left(1 + \frac{1}{2}\right) \frac{(x^2/4)^2}{(2!)^2} + \left(1 + \frac{1}{2} + \frac{1}{3} + \frac{1}{4}\right) \\ &\quad \times \frac{(x^2/4)^4}{(4!)^2} - \dots, \end{aligned} \quad (6c)$$

$$\begin{aligned} \text{kei } x &= -\left[\ln\left(\frac{x}{2}\right) + \gamma\right] \text{bei } x - \frac{\pi}{4} \text{ber } x + \frac{x^2/4}{(1!)^2} \\ &\quad - \left(1 + \frac{1}{2} + \frac{1}{3}\right) \frac{(x^2/4)^3}{(3!)^2} + \dots, \end{aligned} \quad (6d)$$

where  $\gamma$  is the Euler constant,  $\gamma = 0.57721 56649 01532 \dots$ . Four continuity conditions, describing the link from ring  $n$  to next ring  $n + 1$ , allow for determination of the unknowns  $C_{1,n} - C_{4,n}$  from which the determination of  $C_{5,n}$  is directly obtained from the continuity of the displacements. Except for this latter coefficient, which is unnecessary to the determination of the thickness distribution, let us consider the remaining four continuity conditions at segment links: the slope, the radial bending moment, the radial tension, and the tangential elongation. After simplifications, we obtain<sup>19</sup>

(i) slopes:

$$\sum_{i=1}^4 C_{i,n} \frac{d\psi_i}{dx} = \text{invariant for } n \rightarrow n+1; \quad (7a)$$

(ii) radial moments:

$$l_n^5 \sum_{i=1}^4 C_{i,n} \left( \frac{d^2\psi_i}{dx^2} + \frac{\nu}{x} \frac{d\psi_i}{dx} \right) = \text{inv.}; \quad (7b)$$

(iii) radial tensions:

$$l_n^3 \left( \sum_{i=1,3} C_{i,n} \frac{d\psi_{i+1}}{dx} - \sum_{i=2,4} C_{i,n} \frac{d\psi_{i-1}}{dx} \right) = \text{inv.}; \quad (7c)$$

(iv) tangential elongations:

$$l_n \left[ \sum_{i=1,3} C_{i,n} \left( \frac{d^2\psi_{i+1}}{dx^2} - \frac{\nu}{x} \frac{d\psi_{i+1}}{dx} \right) - \sum_{i=2,4} C_{i,n} \left( \frac{d^2\psi_{i-1}}{dx^2} - \frac{\nu}{x} \frac{d\psi_{i-1}}{dx} \right) - (1-\nu) \frac{pl_n^3}{2D_n} \right] = \text{inv.}; \quad (7d)$$

where the sums in the two latter conditions apply only to written values of  $i$ . The first segment  $n=1$  at the mirror vertex is not a ring but a meniscus, then  $C_{3,1} = C_{4,1} = 0$ , which means that no hole exists in this segment. Since the functions  $\psi_1(0) = \text{ber}(0) = 1$  and  $\psi_2 = \text{bei}(0) = 0$ , the setting of the mirror vertex as the origin of the flexure  $z_{\text{flex}}$  is achieved if  $C_{5,1} = -C_{1,1}$ . The two remaining unknowns  $C_{1,1}$  and  $C_{2,1}$  are determined from the link to the next ring,  $n=2$ . The optical ring  $n=N$  extends from  $r_{N-1}$  to  $r_N$ , and is built into a thicker outer segment  $N+1$ . The last segment  $N+1$  is not optically used. If considered as a cylinder, it also requires the determination of four unknowns  $C_{i,N+1}$ . Two of them allow the link with inner ring  $N$ ; the two remaining coefficients describe the external boundaries, i.e., the supporting conditions of a whole mirror.

In a vase form, the boundaries of the outer segment are derived from the deformation of a cylinder<sup>24</sup> with a simply supported rear side. With a meniscus form, the radial thickness of the outer segment is set very small. In both cases the support is realized by an enclosure plate, allowing for the generation of a partial vacuum on the substrate surface.

The orthogonal components of displacements  $w, u$  allow the determination of axial and radial displacements in the original cylindrical coordinate frame. These components are

$$\delta z = w \cos \tan^{-1} \left( \frac{r}{\langle R \rangle} \right) + u \sin \tan^{-1} \left( \frac{r}{\langle R \rangle} \right), \quad (8a)$$

$$\delta r = -w \sin \tan^{-1} \left( \frac{r}{\langle R \rangle} \right) + u \cos \tan^{-1} \left( \frac{r}{\langle R \rangle} \right). \quad (8b)$$

The flexure  $z_{\text{flex}}$  of the middle surface is represented by

$$z_{\text{flex}}\{r + \delta r\} = \delta z. \quad (9a)$$

Using a polynomial smoothing, the flexure can be represented by an even series of the form

$$z_{\text{flex}}\{r\} = \sum_{i=1,2,3,\dots}^{\infty} a_{2i} r^{2i}. \quad (9b)$$

For a shell with  $n$  segments, the above representation is still valid, and an accurate determination of  $a_{2i}$  coefficients requires at least taking into account the flexure of one point per segment, therefore solving an  $n$ -unknown equation system. If we assume that the largest of thicknesses  $\{t_n\}$  is negligible compared to  $\langle R \rangle$ , then the flexure at the mirror surface is the same as that of the middle surface.

Given a thickness distribution  $\{t_n\}$  of  $N$  optical rings, a system of  $4(N+1)$  equations has to be solved to determine the flexure  $z_{\text{flex}}$ . In summary,

$$\{t_n\} \rightarrow C_{i,n} \rightarrow \{w_n\}, \{u_n\} \rightarrow z_{\text{flex}}(r).$$

Given a flexure  $z_{\text{flex}}(r)$  to be achieved, the inverse problem has to be solved to determine the associated  $\{t_n\}$  distribution. Starting from a constant thickness shell, this can be obtained by convenient iterations in varying the distribution  $\{t_n\}$  to obtain the required flexure  $z_{\text{flex}}(r)$ . A dedicated code has been elaborated for this purpose. In a final stage, the solution  $\{t_n\}$  is transformed into  $t_2(r)$  for practical realization of the thickness distribution onto the rear side of the mirror.

The aspherization process generating the optical figure from the flexure of a spherical surface is defined from the coaddition

$$z_{\text{opt}} = z_{\text{sph}} + \varphi z_{\text{flex}}, \quad (10)$$

where  $\varphi$  represents the sign  $+1$  or  $-1$  of the two possible processes that generate an identical optics solution, that is, stress polishing or *in situ* stressing. With these two possible ways of providing an identical solution, the product  $\varphi \times \text{sign}(z_{\text{flex}})$  is the same. With MINITRUST mirrors, all obtained from spherical polishing, we selected for the  $M_2$  substrate the aspherization process by stress polishing and for the  $M_1$ - $M_3$  substrate we selected the aspherization process by *in situ* stressing.

A. Design of the  $M_1$  Substrate with a Single Vase Form

First, the elasticity design of the primary is carried out as a single vase-form mirror. The geometry and

**Table 2. Thickness Distribution of the M<sub>1</sub> Substrate—Single Vase Form**

<i>n</i>	1	2	3	4	5	6	7	8	9	10	11
<i>r</i>	22	44	66	88	110	132	154	176	198	220	240
<i>t<sub>n</sub></i>	20.150	20.166	20.195	20.239	20.299	20.374	20.463	20.565	20.674	20.783	
<i>t<sub>z1</sub></i>	20.150	20.168	20.201	20.251	20.317	20.402	20.502	20.617	20.741	20.868	68

Note: Zerodur:  $\nu = 0.240$ ,  $E = 920 \times 10^3 \text{ kgf/cm}^2$ .  $\langle R \rangle = 2319.5 \text{ mm}$ . Load  $p = -0.8 \text{ kgf/cm}^2$ . Dimensions in mm.

variable thickness distribution of the M<sub>1</sub> substrate is obtained by using a Zerodur–Schott vitrocera. Our sign convention for elasticity and coaddition of profiles requires the opposite sign of that of the optical mirrors in Table 1 and  $z_{\text{sph}} > 0$ . An air depressurization inside the substrate, corresponding to a load  $p < 0$ , provides  $z_{\text{flex}} < 0$ , so we set  $\phi = -1$  and then select an *in situ* stressing at the telescope for the aspherization. The result from the iteration process allows us to determine the M<sub>1</sub> geometry, that is, the curvilinear thickness unknowns  $\{t_n\}$  from which the distribution  $\{t_z\}$  of their projection to the  $z$  axis is derived (Table 2).

The iterations were performed with ten circular rings, where the last ring is built into a thicker outer ring receiving the perimeter reaction at its rear side as centered around the circle  $r = 226 \text{ mm}$ . This outer ring is in a simply supported boundary around this circle, thus avoiding any bending moment at the edge. The resulting mirror profile is the sum of

$$\begin{aligned}
 z_{1 \text{ sph}} &= 0.223 \ 984 \times 10^{-3} r^2 + 0.112 \ 371 \times 10^{-10} r^4 \\
 &\quad + 0.112 \ 750 \times 10^{-17} r^6 + 0.141 \ 414 \\
 &\quad \times 10^{-24} r^8, \\
 \phi z_{1 \text{ flex}} &= 0.002 \ 463 \times 10^{-3} r^2 - 0.176 \ 276 \times 10^{-10} r^4 \\
 &\quad - 0.144 \ 077 \times 10^{-17} r^6 - 0.141 \ 414 \\
 &\quad \times 10^{-24} r^8, \\
 z_{1 \text{ sum}} &= 0.226 \ 448 \times 10^{-3} r^2 - 0.639 \ 050 \times 10^{-11} r^4 \\
 &\quad - 0.313 \ 270 \times 10^{-18} r^6 + 0.201 \ 621 \\
 &\quad \times 10^{-51} r^8, \\
 z_{1 \text{ opt}} &= 0.226 \ 448 \times 10^{-3} r^2 - 0.639 \ 050 \times 10^{-11} r^4 \\
 &\quad - 0.313 \ 270 \times 10^{-18} r^6 + 0.000 \ 000 \\
 &\quad \times 10^{+00} r^8, \tag{11}
 \end{aligned}$$

providing the radius of curvature of the polished sphere  $R_{1 \text{ sph}} = 2232.30 \text{ mm}$ .

**B. Design of the M<sub>3</sub> Substrate with a Single Vase Form**

The elasticity design of the tertiary is also carried out by considering a vase form, but with additional conditions that (i) its perimeter is linked at its edge of radius  $r_l = 90 \text{ mm}$  to the primary and (ii) its edge follows the flexural rotation of the primary. The latter condition is in agreement with the optical design in Table 1, which provides the equality of slopes at this radius and characterizes a modified Rumsey. The M<sub>3</sub> geometry resulting from iterations with the theory of shells is defined by Table 3.

To satisfy the continuity condition for slopes  $z_{1 \text{ opt}}' = z_{3 \text{ opt}}'$  at the link radius  $r = r_l$ , the coaddition must include the rotation  $z_{\text{rota}}$  due to the flexural deformation of M<sub>1</sub> at this radius. A bending moment applied at the perimeter of a constant thickness meniscus provides a purely quadratic flexure. Since the  $t_{z3}$  variation is smaller than 1%, this flexural rotation is accurately taken into account by considering  $z_{\text{rota}} \propto r^2$ . Then the optics profile results from the sum of the following three terms:

$$z_{\text{opt}} = z_{\text{sph}} + \phi z_{\text{flex}} + z_{\text{rota}}, \tag{12}$$

with

$$z_{\text{rota}} = \frac{\phi}{2r_l} \left( \frac{dz_{1 \text{ flex}}}{dr} \right)_{r=r_l} r^2. \tag{13}$$

Since the M<sub>3</sub> sag is much smaller than that of the M<sub>1</sub>, the theory of plates becomes equivalent to the theory of shells for the tertiary analysis. The theory of plates shows that a rotation applied at the edge of a plate, M<sub>3</sub>, by a bending moment generates a purely quadratic flexure. Then the result from iterations, corresponding to data in Table 3, is

**Table 3. Thickness Distribution of the M<sub>3</sub> Substrate—Single Vase Form**

<i>n</i>	1	2	3	4	5	6	7	8	9	10	11
<i>r</i>	1	18	27	36	45	54	63	72	81	90	built-in
<i>t<sub>n</sub></i>	12.042	12.044	12.047	12.052	12.059	12.068	12.078	12.091	12.106	12.122	
<i>t<sub>z3</sub></i>	12.042	12.044	12.048	12.053	12.061	12.070	12.082	12.096	12.112	12.130	$\infty$

Note: Zerodur:  $\nu = 0.240$ ,  $E = 920 \times 10^3 \text{ kgf/cm}^2$ .  $\langle R \rangle = 2294.0 \text{ mm}$ . Load  $p = -0.8 \text{ kgf/cm}^2$ . Dimensions in mm.

Table 4. Geometry of the M<sub>1</sub>-M<sub>3</sub> Global Substrate—Double Vase Form

<i>r</i>	0	18	36	45	54	63	72	81	90 <sup>-</sup>	
<i>t</i> <sub>z13</sub>	12.042	12.044	12.053	12.061	12.070	12.082	12.096	12.112	12.130	
<i>r</i>	90	110	110 <sup>+</sup>	132	154	176	198	220 <sup>-</sup>	220	240
<i>t</i> <sub>z13</sub>	30.190	30.183	20.317	20.402	20.502	20.617	20.741	20.868	68	68

Note: Zerodur vitroceraam:  $\nu = 0.240$ ,  $E = 920 \times 10^3 \text{ kgf/cm}^2$ . Load  $p = -0.8 \text{ kgf/cm}^2$ . Dimensions in mm.

$$\begin{aligned}
 z_{3 \text{ spher}} &= 0.223\,984 \times 10^{-3} r^2 + 0.112\,371 \times 10^{-10} r^4 \\
 &\quad + 0.112\,750 \times 10^{-17} r^6 + 0.141\,414 \\
 &\quad \times 10^{-24} r^8, \\
 \phi z_{3 \text{ flex}} &= 0.001\,400 \times 10^{-3} r^2 - 0.870\,471 \times 10^{-10} r^4 \\
 &\quad + 0.680\,245 \times 10^{-16} r^6 - 0.141\,414 \\
 &\quad \times 10^{-24} r^8, \\
 z_{3 \text{ rota}} &= 0.002\,178 \times 10^{-3} r^2 + 0 + 0 + 0, \\
 z_{3 \text{ SUM}} &= 0.227\,562 \times 10^{-3} r^2 - 0.758\,100 \times 10^{-10} r^4 \\
 &\quad + 0.691\,520 \times 10^{-16} r^6 + 0.139\,328 \\
 &\quad \times 10^{-48} r^8, \\
 z_{3 \text{ opt}} &= 0.227\,562 \times 10^{-3} r^2 - 0.758\,100 \times 10^{-10} r^4 \\
 &\quad + 0.691\,520 \times 10^{-16} r^6 + 0.000\,000 \\
 &\quad \times 10^{+00} r^8, \tag{14}
 \end{aligned}$$

with the same radius of curvature of the polished sphere and load of M<sub>1</sub>, 2232.30 mm and  $-0.80 \text{ kgf/cm}^2$ , respectively.

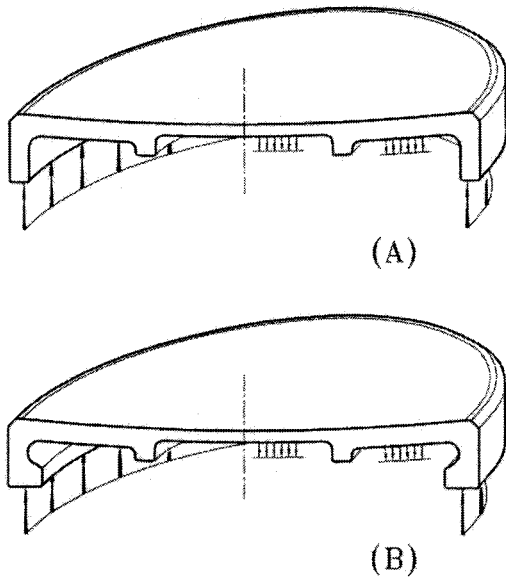


Fig. 5. Elasticity design of the M<sub>1</sub>-M<sub>3</sub> double vase form. Design (A), according to Table 4; design (B), equivalent to design (A) but more compact with an L-shaped outer ring.

### C. Design of a Global Substrate Linking M<sub>1</sub> and M<sub>3</sub>

To realize the geometry of a global substrate in a double vase form, let us define  $r_{1 \text{ min}}$  and  $r_{1 \text{ max}}$  as the inner and outer radii of the M<sub>1</sub> clear aperture. The global substrate must provide the same M<sub>1</sub> flexure as that previously obtained with its single vase form. This can be obtained from the insertion of an intermediate ring by setting  $r_{1 \text{ min}}$  slightly larger than  $r_l$ . The M<sub>1</sub> flexure is recovered by the intermediate ring if its thickness is larger than that of the M<sub>1</sub> proximity. Since the sag at the intermediate ring is low compared with the M<sub>1</sub> sag at its edge, the theory of plate accurately applies to this determination. With  $r_l = 90 \text{ mm}$  and  $r_{1 \text{ min}} = 110 \text{ mm}$ , we obtain the curvilinear thickness  $t_n = 30.220 \text{ mm}$  for the intermediate ring. The final geometry of the M<sub>1</sub>-M<sub>3</sub> double vase design is summarized in Table 4 and displayed in Fig. 5.

Two identical global substrates in a Schott standard Zerodur have been realized by diamond tooling (Fig. 6). The more compact design (B) was selected and two samples were shaped, with an L-shaped outer ring of 204 mm inner radius from blanks available at LOOM for recycling. After spherical polishing without stress, the aspherization of both mirrors was achieved by a closure metal plate and air depressurization corresponding to a uniform load  $p = -0.80 \text{ kgf/cm}^2$ . Fizeau fringes of the simultaneous aspherizations by *in situ* stress were obtained (Fig. 7).

### 4. Elasticity Design of the M<sub>2</sub> Tulip Form by Stress Polishing

Convex hyperboliclike mirrors, such as those used in two mirror telescopes, can be readily obtained by stress polishing using air depressurization during

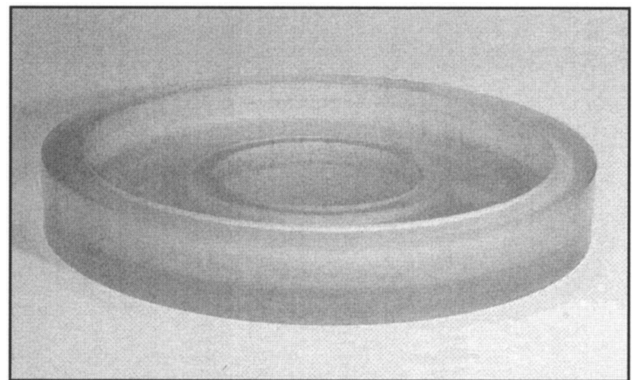


Fig. 6. Rear view of the M<sub>1</sub>-M<sub>3</sub> double vase form.

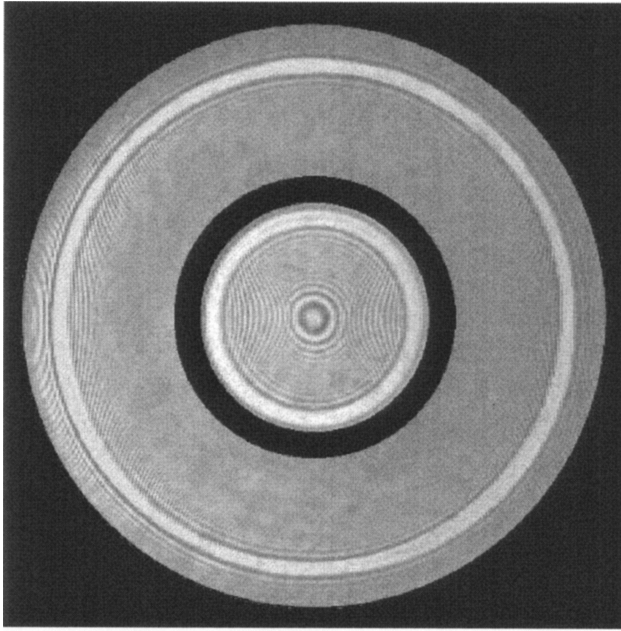


Fig. 7. He-Ne Fizeau interferograms of  $M_1$  and  $M_3$ . For each mirror the autocollimation is achieved at  $\sqrt{3}/2$  of its clear aperture radius  $r_{\max}$  with respect to a sphere. These are  $r_{1\max} = 220$  and  $r_{3\max} = 90$  mm. From the  $M_1$  interferogram, the source is moved 13.32 mm toward the substrate to get the  $M_3$  interferogram.

spherical polishing. Using the vase form, the aspherization process was developed for several telescope secondaries among which is the secondary of the Thémis 1 m Ritchey-Christien at Canaries.<sup>26</sup>

Due to the central hole of the MINITRUST secondary, and to avoid adding central obstruction to the incident beams at primary, it has been interesting to develop an elasticity design with the tulip form.<sup>4,5</sup> This form belongs to the class of variable thickness distributions (VTD) resulting from a force applied at the center for a substrate without a hole. With this class we obtain a theoretical axial thickness  $t_z(0) \rightarrow \infty$ , which can be limited to a finite value in accordance with a small flexure residual within the Rayleigh criterion. Considering the MINITRUST secondary, this form leads to a substrate starting with a rigid ring around the central aperture, continuing with a decreasing thickness for the clear aperture area, and ending with a null thickness. With this free edge solution, the outer diameter of the tertiary can be just a little larger than the tertiary clear aperture, which is also the telescope pupil (see Table 1). A

uniform load  $p$  is applied to the rear area of the substrate while the reacting ring force is located at the rear side edge of the central rigid ring. For this, a Zerodur central meniscus is mounted, simply supported at its edge to close the rigid ring hole at the optical side, thus also providing a better surface continuity of the polishing. An outside metal cylinder reaching the level of the  $M_2$  edge provides the enclosure for a partial vacuum by use of a waterproof paste. The shearing force  $Q_r$ , corresponding to this loading configuration, is represented by

$$Q_r = \frac{p}{2} \left( 1 - \frac{r^2}{r_{\text{ext}}^2} \right) r, \quad (15)$$

where the free edge radius  $r_{\text{ext}}$  is a little larger than the outer clear aperture radius  $r_{\max}$ .

The flexure is determined from the difference between the polishing sphere and the optical  $M_2$  figure in Table 5. By stress polishing, the coaddition is represented by

$$z_{\text{opt}} = z_{\text{sph}} + z_{\text{flex}}, \quad (16)$$

and the built-in condition at the inner clear aperture radius entails identical slopes between  $z_{\text{opt}}$  and  $z_{\text{sph}}$  at this radius,

$$dz_{\text{sph}}/dr \big|_{r_{\min}} = dz_{\text{opt}}/dr \big|_{r_{\min}}, \quad (17)$$

which fully defines the radius of curvature  $R_{\text{sph}}$  of the figuring tools, and then the elastic deformation to generate  $z_{\text{flex}}$ .

Assuming that the middle surface of the substrate clear aperture will appear relatively flat, the theory of thin plates applies to the determination of the  $M_2$  VTD. The boundaries are defined from the following: (a) a bounded central meniscus of radius  $r_{\text{int}}$  closing the central hole for the polishing and also to improve the built-in condition; (b) a constant thickness rigid ring from  $r_{\text{int}}$  to  $r_{\min}$ ; and (c) a VTD to be determined, which is built in at the ring outer radius corresponding to the  $M_2$  inner clear aperture radius  $r_{\min}$  and expanding up to the free edge of radius  $r_{\text{ext}}$ , which is a little larger than the outer clear aperture radius  $r_{\max}$ . The rigidity  $D(r) = Et(r)^3/12(1 - \nu^2)$  is determined by integration of the derivative equation

Table 5. Thickness Distribution of the  $M_2$  Substrate—Tulip Form

$r$	30	50	50 <sup>+</sup>	60	70	80	85	90	95	100	103
$t_{z2}$	32.000	31.273	14.343	9.997	7.108	4.896	3.926	2.999	2.069	1.042	0.308 <sup>a</sup>
$z_B^b$			9.318	5.471	3.173	1.641	1.044	0.512	0.200	0.000	0.000

Note: Zerodur vitrocera:  $\nu = 0.240$ ,  $E = 920 \times 10^3$  kgf/cm<sup>2</sup>. Load  $p = -0.8$  kgf/cm<sup>2</sup>. Dimensions in mm. Clear aperture radii  $r_{\min} = 50$  and  $r_{\max} = 100$ . Outer edge  $r_{\text{ext}} = 103$ . Maximum stress 64 kgf/cm<sup>2</sup>.

<sup>a</sup>Avoiding zero for a practical realization, this thickness is finally set from the tangent at  $t(r_{\max})$ .

<sup>b</sup> $z_B$  represents the shape of the rear surface without stress and includes the flexure overthickness for diamond tooling. The rear surface ends flat toward the edge.

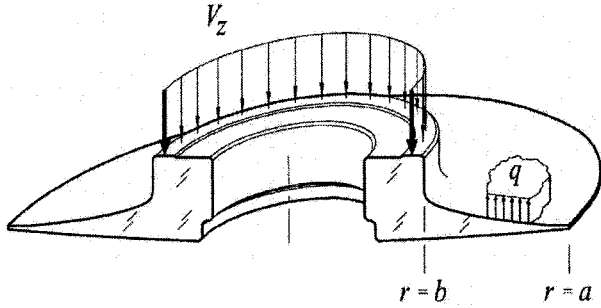


Fig. 8. Elasticity design of the  $M_2$  substrate.

$$D \frac{d}{dr} \left( \frac{d^2 z}{dr^2} + \frac{1}{r} \frac{dz}{dr} \right) + \frac{dD}{dr} \left( \frac{d^2 z}{dr^2} + \frac{\nu}{r} \frac{dz}{dr} \right) = Q_r, \quad (18)$$

where  $z \equiv z_{\text{flex}}$ . The numerical integration is carried out from  $r_{\text{min}}$  toward increasing radius with a small increment  $dr$ , starting with a provisional value of the thickness  $t_{z_2}(r_{\text{min}})$ . The process is repeated by changing the starting thickness to obtain a null thickness at edge  $r_{\text{ext}}$ . Then the radial increment is decreased and the process repeated to provide a convenient accuracy. The resulting VTD for a uniform load  $p = -0.80 \text{ kgf/cm}^2$  is displayed by Table 5.

Using an opposite sign convention for the optical surface  $z_{2\text{opt}}$  represented in Section 2, the coaddition providing the secondary mirror shape and associated with its thickness geometry in Table 5 is represented by the series set

$$\begin{aligned} z_{2\text{sph}} &= 0.454\,340 \times 10^{-3} r^2 + 0.937\,868 \times 10^{-10} r^4 \\ &\quad + 0.387\,198 \times 10^{-16} r^6 + 0.199\,820 \\ &\quad \times 10^{-23} r^8, \\ \varphi z_{2\text{flex}} &= 0.001\,864 \times 10^{-3} r^2 - 0.373\,737 \times 10^{-09} r^4 \\ &\quad + 0.203\,131 \times 10^{-15} r^6 - 0.199\,521 \\ &\quad \times 10^{-23} r^8, \\ z_{2\text{SUM}} &= 0.456\,204 \times 10^{-3} r^2 - 0.279\,950 \times 10^{-09} r^4 \\ &\quad + 0.241\,851 \times 10^{-15} r^6 + 0.299\,163 \\ &\quad \times 10^{-26} r^8, \\ z_{2\text{opt}} &= 0.456\,204 \times 10^{-3} r^2 - 0.279\,950 \times 10^{-09} r^4 \\ &\quad + 0.241\,840 \times 10^{-15} r^6 + 0.000\,000 \\ &\quad \times 10^{+00} r^8, \end{aligned} \quad (19)$$

where the  $r^8$  term of  $z_{2\text{SUM}}$  is negligible. The resulting radius of curvature of the figuring sphere is  $R_{\text{sph}} = 1100.50 \text{ mm}$ .

The final design of the  $M_2$  substrate (Fig. 8) provides a light mirror, which is useful for space telescopes. As for the  $M_1$ – $M_3$  substrate built in two samples, three  $M_2$  substrates were shaped by the Cybernetix Corporation, using diamond tooling with

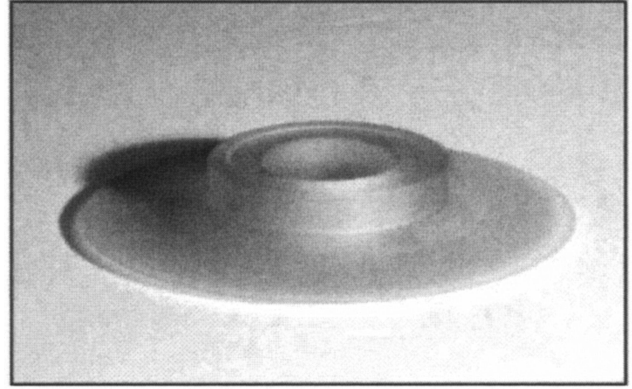


Fig. 9. Rear view of the  $M_2$  tulip form.

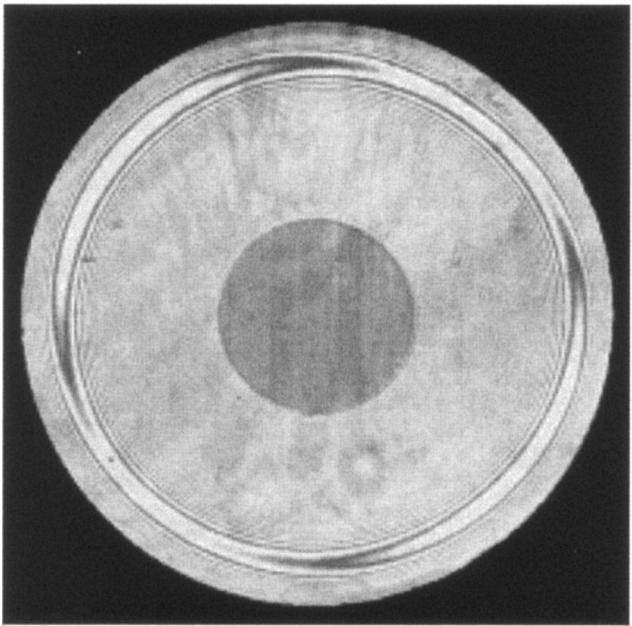
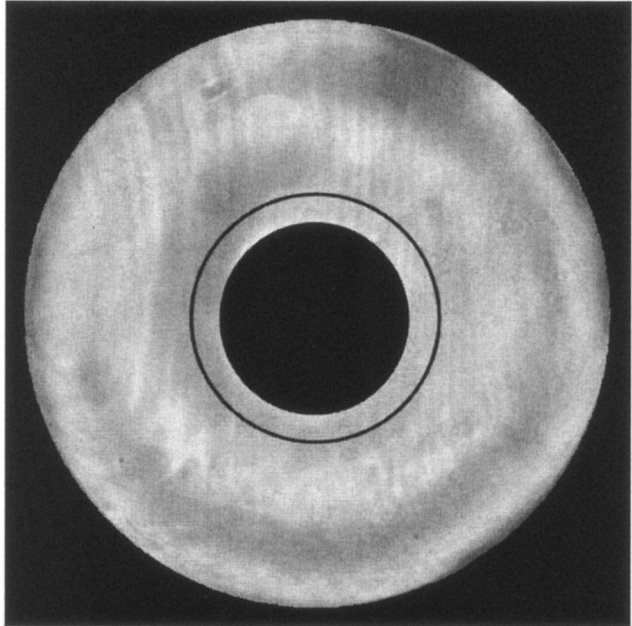


Fig. 10. He–Ne Fizeau interferograms of  $M_2$ . Top, mirror shape during stress; bottom, shape after elastic relaxation.

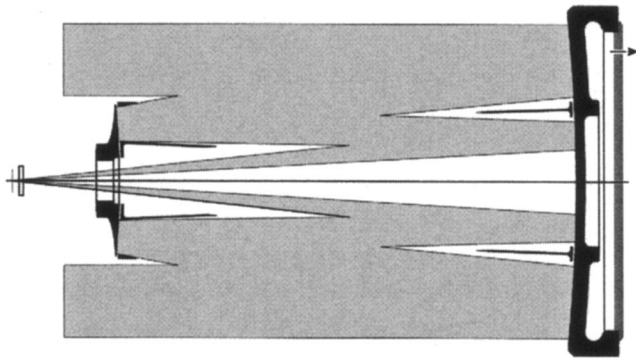


Fig. 11. MINISTRUST on-axis beam and substrates. The entrance pupil is on  $M_2$ .

a computer-controlled machine (Fig. 9). Interferograms of the mirror shape during stress and of its final shape after elastic relaxation are displayed in Fig. 10. With ground-based telescopes, it can be shown from a comparative study of various thickness profiles<sup>27</sup> that such a large secondary mirror with a tulip form—probably up to 1 m diameter—can be supported only at the level of its inner ring without significant deformation due to the Earth's gravity, which would alter its optical shape.

### 5. Telescope Optical Tests in the Laboratory

The thickness configurations of the three mirrors  $M_1$ ,  $M_2$ , and  $M_3$  together with the on-axis incident and reflected beams and the baffles are displayed in Fig. 11.

Two samples of the telescope optics have been built for MINISTRUST-1 and -2. With MINISTRUST-1, a telescope tube of the Serrurier type was realized to avoid the flexural rotations of the mirrors from the tube deformation during its motions. In a first stage, since the cocentering of  $M_1$  and  $M_3$  is *de facto* realized with high accuracy by the single substrate in a double vase, the telescope axis was set up by retroreflection of a He–Ne laser beam at the  $M_3$  vertex by the center of the telescope head ring materialized by a wire reticle. Then the lateral cocentering and rotations of

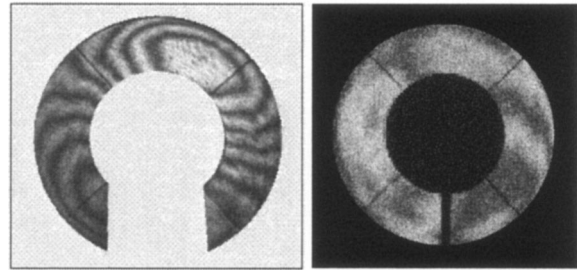


Fig. 13. MINISTRUST-1 He–Ne wave front after a telescope double pass. Left: decentering coma before the  $M_2$  setup, right: after the  $M_2$  setup.

$M_2$  in  $x$  and  $y$  was realized from this laser beam retroreflecting onto the  $M_3$  vertex by the  $M_2$  vertex, which was represented by a cross on a glass plate accurately mounted onto its central hole to observe the image of a diffraction cross.

The final test was performed by autocollimation with a Fizeau interferometer imaging a point source at the telescope focus. The telescope output beam was reflected by a plane mirror and was passed a second time in the telescope (Fig. 12). From data reductions of the wavefronts issued from a double pass through the telescope, the final *in situ* load at  $M_1$ – $M_3$  is  $0.794 \text{ kgf/cm}^2$ ; the theoretical value was  $0.8 \text{ kgf/cm}^2$ . The first double-pass He–Ne interferogram [Fig. 13 (left)] displays a dominating *Coma*<sub>3</sub>, here balanced by *Tilt*<sub>1</sub> due to the decentering of  $M_2$ . This was nulled by a convenient centering of  $M_2$  [Fig. 13 (right)]. The final data reduction from the phase-shift interferometer gave the following peak-to-valley (ptv) residuals onto the wavefront issued from the double pass:

$$Sphe3 = 0.06 \lambda, \quad Coma3 = 0.07 \lambda,$$

$$Astm3 = 0.42 \lambda.$$

Those errors should be divided by 2 for a wavefront issued from a star; thus the overall sum, including all order aberrations, is  $0.280 \lambda_{\text{He-Ne}}$  ptv corresponding to rms  $0.048 \lambda_{\text{He-Ne}}$ . MINISTRUST-1 should be installed at Haute-Provence Observatory. The second optical set

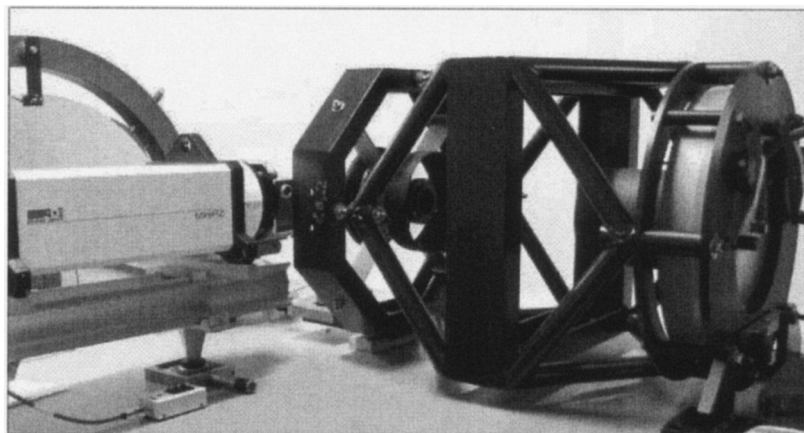


Fig. 12. View of MINISTRUST-1 under alignment and double-pass testing by autocollimation on a plane.

allowed MINISTRUST-2 to be installed in Italy by Ias-Frascati<sup>28</sup> for preliminary demonstrations in the sky.

## 6. Conclusions

The modified-Rumsey form requires use of all the free parameters available for a flat-field anastigmatic three mirror telescope optimization obtained by active optics methods. This leads to the polishing of only two surfaces that are spheres: the combined primary-tertiary mirror and the secondary mirror. To our knowledge, MINISTRUST-1 and -2 are the first telescopes built entirely from active optics methods; stress polishing and *in situ* stressing have both been used. These methods present considerable potential development for providing diffraction-limited images while avoiding zonal errors of high spatial frequency. The vase form and tulip form are in agreement with Saint Venant's principle, since these forms allow the forces to act as far as possible from the optical surface. Hence, near the boundary of the optical surfaces, all slope discontinuities due to the shear component of the flexure are minimized.

Active optics methods also present the capability to obtain off-axis mirrors up to high-order aberration corrections.<sup>1,2</sup> In the present case of axisymmetric optics, 2 or 3 m aperture modified-Rumsey designs will be proposed as survey telescopes for observations from the ground (such as at the Antarctica, Concordia station<sup>29,30</sup>) and also in space.

With only two spherical surfaces to polish, this compact design can provide diffraction-limited field imaging at any wavelength range.

This research and development was partly supported by BQR 98 from the Université de Provence, Aix-Marseille I.

## References and Note

- G. R. Lemaître, "Active optics: vase or meniscus multimode mirrors and degenerated monomode configurations," *Mechanica* **40**, 233–249 (2005).
- G. R. Lemaître, "Active optics and aberration correction with multimode deformable mirrors (MDMs)—vase form and meniscus form," in *Laser Optics 2003*, V. E. Sherstobitov and L. N. Soms, eds., Proc. SPIE **5481**, 70–81 (2003).
- G. R. Lemaître, "New procedure for making Schmidt corrector plates," *Appl. Opt.* **11**, 1630–1636 (1972).
- G. R. Lemaître, "Active optics and elastic relaxation methods," in *Current Trends in Optics*, International Commission for Optics 12 (Taylor & Francis, London, 1981), pp. 135–149.
- G. R. Lemaître, "Various aspects of active optics," in *Telescopes and Active Systems*, F. Roddier, ed., Proc. SPIE **1114**, 328–341 (1989).
- M. C. E. Huber, E. Jannitti, G. R. Lemaître, and G. Tondello, "Toroidal grating obtained on elastic substrate: SOHO Mission," *Appl. Opt.* **20**, 2139–2142 (1981).
- M. Ferrari, "Development of variable curvature mirrors for the delay lines of the VLTI," *Astron. Astrophys. Suppl. Ser.* **128**, 221–227 (1998).
- J. Lubliner and J. E. Nelson, "Stressed mirror polishing. 1: A technique for producing nonaxisymmetric mirrors," *Appl. Opt.* **19**, 2332–2340 (1980).
- J. E. Nelson, G. Gabor, L. K. Hunt, J. Lubliner, and T. S. Mast, "Stressed mirror polishing. 2: Fabrication of an off-axis section of a paraboloid," *Appl. Opt.* **19**, 2341–2350 (1980).
- H.-J. Su and X. Cui, "Lamost project and its current status," in *Large Ground-Based Telescopes*, J. M. Oschmann and L. M. Stepp, eds., Proc. SPIE **4837**, 26–35 (2003).
- R. N. Wilson, "Active optics control systems," in *Reflecting Telescope Optics II* (Springer, Berlin, 1999), pp. 274–314.
- G. Schwesinger, "Nondistorting lateral edge support of large telescope mirrors," *Appl. Opt.* **33**, 1198–1202 (1994).
- L. Noethe, "Active optics in modern large optical telescopes," in *Progress in Optics, Vol. XLIII*, E. Wolf, ed. (Elsevier-North-Holland, Amsterdam, 2002), pp. 1–69.
- N. J. Rumsey, "A compact three-reflection astronomical camera," in *Optical Instruments and Techniques, Ico 8 Meeting*, London, H. Dickson, ed. (Oriel, Newcastle, 1969), pp. 514–520.
- R. V. Willstrop, "The Mersenne-Schmidt: a three reflection survey telescope," *Mon. Not. R. Astron. Soc.* **210**, 597–609 (1984).
- M. Paul, "Systèmes correcteurs pour réflecteurs astronomiques," *Rev. Opt. Theor. Instrum.* **14**, 169–202 (1935).
- J. R. P. Angel, N. J. Woolf, and H. W. Epps, "A 1.8-m three mirror telescope proposal for survey with CCDs," in *Advanced Technology Optical Telescopes*, G. Burbidge and L. Barr, eds., Proc. SPIE **332**, 134–142 (1982).
- K. Dohlen, M. Saisse, G. Claeysen, P. Lamy, and J.-L. Boit, "Optical designs for the Rosetta camera," *Opt. Eng.* **35**, 1150–1157 (1996).
- G. R. Lemaître and M. Wang, "Optical results with segmented Témos 4," in *Metal Mirrors*, R. G. Bingham and D. D. Walker, eds., Proc. SPIE **1931**, 43–52 (1992).
- G. R. Lemaître, "A diffraction limited 20 m telescope with an active and adaptive tertiary," in *Advanced Technology Optical/IR Telescopes*, L. N. Stepp, ed., Proc. SPIE **3352**, 766–777 (1998).
- E. Reissner, "General theory of shallow spherical shells—I," *J. Math. Phys. (Cambridge, Mass.)* **25**, 80–85 (1946).
- E. Reissner, "General theory of shallow spherical shells—II," *J. Math. Phys. (Cambridge, Mass.)* **25**, 279–300 (1947).
- H. B. Dwight, in *Table of Integrals and Other Mathematical Data*, 3rd ed. (Macmillan, New York, 1957), pp. 184–188, 276–279.
- M. Abramovitz and I. A. Stegun, eds., *Handbook of Mathematical Functions* (Dover, New York, 2003), pp. 374–384 and 430–431.
- S. P. Timoshenko and S. Woinowsky-Kieger, in *Theory of Plates and Shells* (McGraw-Hill, New York, 1959), pp. 558 and 466. Note: In this book, the following representation is used for the  $\psi_i$  functions:  $\psi_1 = \text{ber}$ ,  $\psi_2 = -\text{bei}$ ,  $\psi_3 = -(2/\pi)\text{kei}$ ,  $\psi_4 = -(2/\pi)\text{ker}$  on p. 560 and in the Tables on pp. 491–494. Reissner (Refs. 20 and 21) represents these functions directly by  $\psi_1 = \text{ber}$ ,  $\psi_2 = \text{bei}$ ,  $\psi_3 = \text{ker}$ ,  $\psi_4 = \text{kei}$ .
- G. Molodij, J. Rayrole, P. Y. Madec, and F. Colson, "Thémis: Télescope héliographique pour l'étude du magnétisme et des instabilités solaires," *Astron. Astrophys. Suppl. Ser.* **118**, 169–179 (1996), and <http://arthemis.na.astro.it/themis>.
- G. R. Lemaître, "Sur la flexion des miroirs secondaires de télescopes," *Nouv. Rev. Opt.* **7**, 389–397 (1976).
- C. D. La Padula, A. Carusi, R. F. Viotti, A. Vignato, and G. R. Lemaître, "Proposal for a mini-satellite with a wide-field TRT," *Mem. Soc. Astron. Ital.* **74**, 63 (2003).
- R. F. Viotti, M. Badiali, A. Boattini, A. Carusi, R. U. Claudi, A. Di Lellis, C. D. La Padula, M. Frutti, A. Vignatto, and G. R. Lemaître, "Wide field observations at Dome C, Antarctica," *Mem. Soc. Astron. Ital. Suppl.* **2**, 177–180 (2003).
- M. Ferrari, G. R. Lemaître, R. F. Viotti, C. La Padula, G. Comtes, M. Blanc, and M. Boer, "Three reflection telescope proposal as flat-field anastigmat for wide field observations at Dome C," in *Astronomie et Astrophysique au Dome C*, Cers Toulouse, Cnrs-Insu Proc., in press (2005).